C Journal of Carbon Research

MDPI

Article

Viability of Activated Carbon Derived from Polystyrene Sulphonate Beads as Electrical Double Layer Capacitors

Gbenro Babajide Folaranmi [1,2,*], Anthony Ekennia [2], Nkiruka Chidiebere Ani [2] and Richard Chukwuemeka Ehiri [2]

[1] Institut Européen des Membranes, IEM, UMR-5635, Université de Montpellier, ENSCM, CNRS, Place Eugène Bataillon, CEDEX 5, 34095 Montpellier, France

[2] Department of Chemistry, Faculty of Physical Sciences, Alex Ekweme Federal University, Ndufu Alike Ikwo, 1010 Abakaliki, Nigeria; chemisttony@gmail.com (A.E.); nkiruoji@yahoo.com (N.C.A.); richcee2003@yahoo.com (R.C.E.)

* Correspondence: gbenro.folaranmi@etu.umontpellier.fr

Abstract: In this paper, a commercial polymeric resin precursor (polystyrene sulphonate beads) was used as a source of carbon spheres. The resin was pyrolyzed at different temperatures (700, 800, and 900 °C) and the resulting carbons were analyzed by cyclic voltammetry (CV) and electrochemical impedance spectroscopy (EIS). From the result of EIS, carbon spheres obtained at 700 °C (CS−700) have the least ohmnic resistance and highest capacitance. In furtherance, the resin was chemically activated with iron (III) chloride $FeCl_3 \cdot 6H_2O$ at different concentration (0.1 M, 0.3 M, and 0.5 M) and pyrolyzed at 700 °C to obtain activated carbon sphere namely (ACS 700−0.1, ACS 700−0.3, and ACS 700−0.5) in which the last digit of the samples denotes the concentration of $FeCl_3$. Scanning electron microscope (SEM) showed that the carbon is of spherical shape; X-ray diffraction (XRD), energy dispersive spectroscopy (EDS), and X-ray photon electron spectroscopy (XPS) revealed successful introduction of Fe on the surface of the carbon. Out of all the activated carbon spheres, ACS 700−0.1 exhibited highest double layer capacitance of 9 μF cm^{-2} and lowest charge transfer resistance of 3.33 KΩ·cm^2. This method shows that carbon spheres obtained from a polymeric source can be easily improved by simple resin modification and the carbon could be a potential candidate for an electrical double layer capacitor.

Keywords: polystyrene sulphonate beads; carbon spheres; capacitors; electrochemical impedance spectroscopy

Citation: Folaranmi, G.B.; Ekennia, A.; Ani, N.C.; Ehiri, R.C. Viability of Activated Carbon Derived from Polystyrene Sulphonate Beads as Electrical Double Layer Capacitors. *C* **2021**, *7*, 82. https://doi.org/10.3390/c7040082

Academic Editors: Lok Kumar Shrestha and Rekha Goswami Shrestha

Received: 21 October 2021
Accepted: 24 November 2021
Published: 26 November 2021

1. Introduction

The field of electrochemical capacitors, with a focus on electrical double layer capacitors (EDLCs), is becoming increasingly popular in our day. Capacitors are energy storage devices that have a fast charging and discharging rate, a high energy density, and a long cycle lifetime [1]. The ion storage mechanism of a supercapacitor/pseudo-capacitor is based on the Faradaic redox process [2], whereas the ion storage mechanism of an EDLC is based on a non-redox process (adsorption process) [3]. Both types of capacitors work on the same principle: two sandwiched electrodes are sandwiched in an electrolyte and set parallel to each other. The electrodes may or may not be separated by membranes, depending on the cell's architecture.

Supercapacitors have been used in the fields of batteries, catalysis, and sensors, among other things [4,5], while EDLCs have been used in the field of desalination, energy storage, etc. [6]. Because of their porosity, high surface area, and adsorption capabilities, carbon-based materials have been widely explored as capacitor sources [7,8]. Carbon, on the other hand, has some downsides—such as low hydrophilicity, low capacitance, and low conductivity, to name a few [9]—and as a result, techniques to overcome these shortcomings have been the focus of recent research.

The use of chemical or physical methods to improve the physico-chemical properties of carbon via doping, additives, thermal annealing [10], freeze drying technique [11], and beam irradiation [12], has been reported in literature. Due to their high porosity, large surface area, and regulated pores arrangement, carbon-based biopolymers such as cellulose and sucrose have recently gained attention as an alternative carbon source to commercial carbon (petrochemical product) [13]. Mao et al. [14] reported sucrose-based carbon with a specific capacitance of 316 F g^{-1}, while Yan et al. [15] published N/S coal-based carbon with a specific capacitance of 301 F g^{-1} in the literature. However, most of these precursors are expensive and hard to come by, necessitating the search for a low-cost alternative.

Carbons, because of their unique features—such as a large specific surface area, varied pore structure, and availability—have a lot of potential for long-term industrial use. Carbon materials with regulated macroscopic forms, such as beads, are, on the other hand, in high demand because they can suit the needs of most industrial applications.

In the literature, various types of functionalized activated carbon beads have been recorded with the goal of addressing specific applications. Steam, CO_2, $ZnCl_2$, and KOH activations [16–19], have all been studied and optimized for the manufacture of carbon materials with high surface areas and appropriate pore topologies for a variety of applications. However, the time and cost of the extensive post-synthesis modification methods prevent practical manufacture of carbon spheres on a wide scale. As a result, great emphasis was placed on making the preparation of activated carbon as simple as possible. By mixing an activating chemical (solid KOH and $ZnCl_2$) with biomass, Singh et al. observed a single-step activation. The synthesized activated biocarbon had a high BET surface area and good porosity, but its shape and particle size were not well characterized [20,21].

There is little or no well-established synthetic approach for producing carbon beads with the appropriate particle size and homogeneous pore size distribution at the moment to the best of our knowledge. As a result, a unique and efficient method of producing porous carbon spheres is very desirable. The usage of shaped polymer beads as a precursor to activated carbon beads is one option that could be pursued. Cation exchange resin beads are the most likely candidate among the industrially available shaped polymer beads to meet these requirements. They can be made in a variety of sizes and pore configurations. Furthermore, they provide evenly distributed ion exchange sites, allowing for the insertion of an activator that promotes the carbonization reaction and, as a result, the pore structure of the carbon beads. Therefore, the goal of this research is to make carbon beads with a well-defined spherical form and a mesoporous structure that could be employed as an EDLC while using resin beads as the starting material because of their acceptable particle size and morphology.

Because of the pore structure of cation exchange resin beads, the activator—in this case iron—is distributed uniformly, resulting in a very uniform carbonization reaction and in order to optimize the pore structure of the resultant carbon beads for surface charge improvement to promote better electron transport within the carbon structure, the resin beads were ion exchanged with $FeCl_3$ solutions of various concentrations and carbonized at 700–900 °C (optimized temperature range for effective carbonization). Carbon spheres with a predetermined shape and size were created, as well as a mesopore network.

Aside from research on naturally occurring polymers—such as sucrose, glucose, and cellulose—synthetic polymers as carbon sources have recently been a subject of recent research in the EDLCs community, and there has been a report on the electrochemical behavior of carbon-based synthetic polymer sources in the literature [22,23]. Intense treatment conditions, such as thermal or hydrothermal breakdown, are required for the synthesis of graphitic carbon from precursory polymers. Due to the significant instability of the polymer backbone, oxygen-rich polymers—particularly those with unsaturated bonds and heteroatoms—have a strong tendency to decompose into carbon when heated. Prior to pyrolysis, the polymer undergoes a crosslinking phase (stabilization), which results in the transformation of the polymer into carbon. Under specific conditions, polymers such as polyacrylonitrile (PAN), polyethylene glycol (PEG), and polyethylene (PE) have been

reported as carbon sources in the literature [24–27]. However, there are few reports in the literature about carbon-derived polystyrene sulphonate beads.

As a result of this, we studied the pyrolytic conditions and electrochemical behavior of carbon generated from this commercial polymeric-based precursor (polystyrene sulphonate beads) through chemical modification of the polymer followed by pyrolysis at various temperatures.

2. Materials and Methods

2.1. Materials

Polymer resin polystyrene sulphonate beads (DOWEX 50WX8-Hydrogen form CAS no: 217492-100G), polyvinylidenefluoride (PVDF) (CAS no. 24937-79-9), N-methyl-2-pyrrolidone (NMP) (CAS no. 872-50-4, 99.7%, M.W 99.13 g/mol), and sodium chloride (NaCl) were all purchased from Sigma Aldrich, Steinheim, Germany. Iron chloride hexahydrate ($FeCl_3 \cdot 6H_2O$) (CAS no. 10625-77-1 99%, M.W 270.30 g/mol) was purchased from Merck, Sigma Aldrich, Germany.

Resin Pyrolysis and Activation

Briefly, 4.5 g of the polymer resin was put in a crucible boat and placed in a hollow tube furnace under pure nitrogen for 2 h at a ramp rate of 3°/min at different temperatures (700, 800, and 900 °C). After pyrolysis, the samples were named after their corresponding temperature—i.e., CS 700, CS 800, and CS 900.

For chemical activation, different molarities of $FeCl_3$ (0.1, 0.3, and 0.5 M) were prepared and impregnated with 4.5 g of the polymer resin. The solution was stirred for 20 h. After, it was filtered, washed with distilled water, and dried overnight at 80 °C. The modified polymer resin was then pyrolyzed at a particular temperature under the same condition as mentioned above.

2.2. Experimental Procedure

Solid Electrode Preparation for CV and EIS Studies

Solid carbon electrode was prepared as a suspension of carbon sphere powder (0.3 g), and poly (vinylidene fluoride PVDF, 0.03 g) in 2 mL N-Methyl-2-pyrrolidone (NMP). The mixture was stirred for 3 h to ensure homogeneity and PVDF dissolution. Few drops of the slurry were then slowly deposited on a graphite sheet area of 1 cm^2. The deposited electrode was dried at 80 °C in an oven for 2 h.

2.3. Physical Characterization

Field emission scanning electron microscopy (FESEM) was used to analyze the morphology of the samples (FESEM, Hitachi S4800, Tokyo, Japan). The structural properties were studied by using Raman spectroscopy (HORIBA Xplora, Minami-ku, Kyoto, Japan). X-ray diffractometer (XRD Pan Analytical X'pert Phillips, Lelyweg, EA, Almelo, The Netherlands) was used to reveal the crystallinity of the materials. Energy dispersive X-ray (EDX Oxford X-Max, Oxford, UK) and X-ray photon electron spectroscopy (XPS) (ESCALAB 250 Thermo Electron, Strasbourg, France) analyses were done to investigate the atomic composition and chemical functional groups (moities) of the materials. For the XPS analysis, the excitation source was a monochromatic source Al Kα anode with photo energy that was observed at 1486.6 eV. The analyzed surface has a diameter of 500 μm. The photoelectron spectra were calibrated in terms of bond energy with respect to the energy of the C=C component of carbon C1s at 284.4 eV and Fourier transmission infer-red (410 ATR FTIR spectrometer) was done to also verify the functional groups present in the materials. Specific surface area was obtained by using N_2 adsorption/desorption at 77 K. S_{BET} was the specific surface area calculated by the Brunauer–Emmett–Teller (BET) method (Micromeritics 2020 ASAP, Merignac, France). Vt was the total pore volume calculated from the amount adsorbed at a relative pressure (P/P°) of 0.99, V_{meso} was the mesopore volume calculated by the Barrett–Joyner–Halenda (BJH) model.

2.4. Electrochemical Characterizations

The electrochemical properties of the as prepared electrodes were examined by electrochemical impedance spectroscopy (EIS) and cyclic voltammetry (CV). EIS was performed using a three-electrode system. The carbon electrode (deposited on a graphite sheet as support) with an exposed surface area of 1 cm^2 was made to have contact with the electrolyte (1 M NaCl solution), platinum mesh and Ag/AgCl served as counter and reference electrodes respectively. The measurement was done with Origalys Potentiostat (OGF01A, Origalys Electrochem SAS, Les Verchères 2, France) at an operating frequency of 1000 KHz to 10 mHz and a sine wave of 10 mV.

Cyclic voltammetry was also performed on Origalys Potentiostat (OGF01A, Origalys Electrochem SAS, Les Verchères 2, France) using a three-electrode system as described above at an operating window of −0.4 to 0.8 V vs. ref (0.1 V Ag/AgCl) in a 1.0 M NaCl electrolyte. The double-layer capacitance (C_{DL}) was determined using cyclic voltammetry at different scan rates by considering the open circuit potential (OCP 0.1 V vs. ref) of the charging and the discharging currents. The determined double-layer capacitance of the system was the absolute value of the slope of the linear plot of charging current fitted to the data. Double-layer capacitance (C_{DL}) is calculated using Equation (1) below

$$i = v\, C_{DL.} \quad (1)$$

For an ideal capacitor Q = CV, thus by differentiation i = C v, where v is the scan rate.

The double-layer charging current i is equal to the product of the scan rate, v, and the electrochemical double-layer capacitance, C_{DL}.

Galvanostat charge discharge (GCD) was also performed on the same system described above at a current density of 0.1 A/g.

3. Results

3.1. SEM Study

The shape of the produced carbon was verified using SEM at various temperatures. The synthesized carbon is spherical in nature with approximately uniform size, as shown in Figure 1a–f. As can be shown in Figure 1 from SEM, carbon spheres obtained at 700 °C are quite smooth after pyrolysis (a–b). Also, at higher temperatures, the resin beads appear to break down or disintegrate more, presumably due to the pressure exerted inside the beads, which causes expansion and uneven decomposition. Using KEYENCE SEM software, the average diameter of the pore size was 140 ± 0.003 µm. Also, following activation, there was no modification in the shape of the carbon spheres (Supplementary Information Figure S1a).

3.2. XRD Studies

XRD was used to investigate the crystal nature of the CS, as shown in Figure 2a. All of the samples show broad diffraction peaks at 2 = 23° and 44.5°, which correspond to the 002 and 100/101 planes of carbon, respectively, which is a typical carbon diffraction peak [28]. The carbon materials are amorphous and low graphitic in nature (display of broad diffraction bands). The temperature of pyrolysis has no effect on the crystallinity of carbon. It was further shown that temperature has no major effect on the inter-planar distance using Bragg's law (n = 2dsinΘ), where n = 1, d is the inter-planar distance, and is the angle of diffraction (d002 and d001) as no much difference is observed as shown in Table 1. The interlayer spacing between two adjacent carbon sheets in a typical carbonaceous material, such as ordered graphite, is 0.335 nm [9]. Our materials have a disordered carbonaceous character, corresponding to an interlayer distance (d002) of 0.377–0.38 nm.

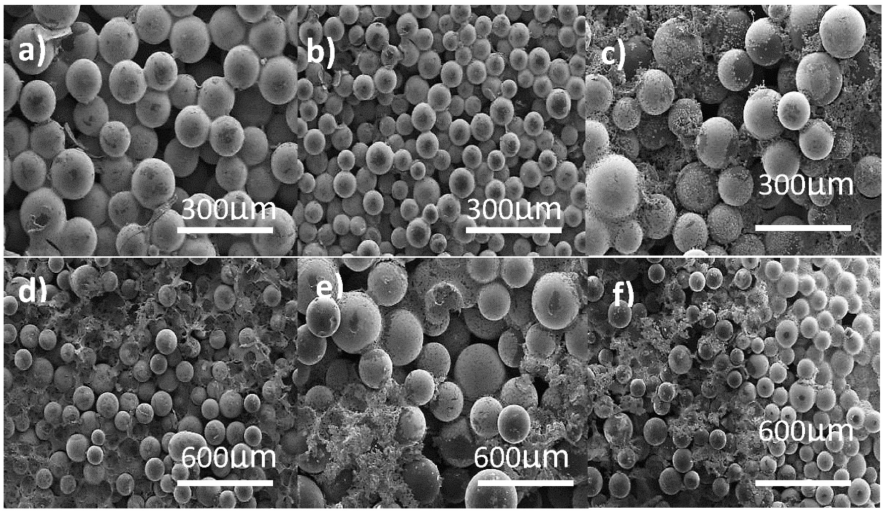

Figure 1. SEM micrographs of carbon spheres (CS) at different magnification scales: (**a**,**b**) CS 700; (**c**,**d**) CS 800; (**e**,**f**) CS 900.

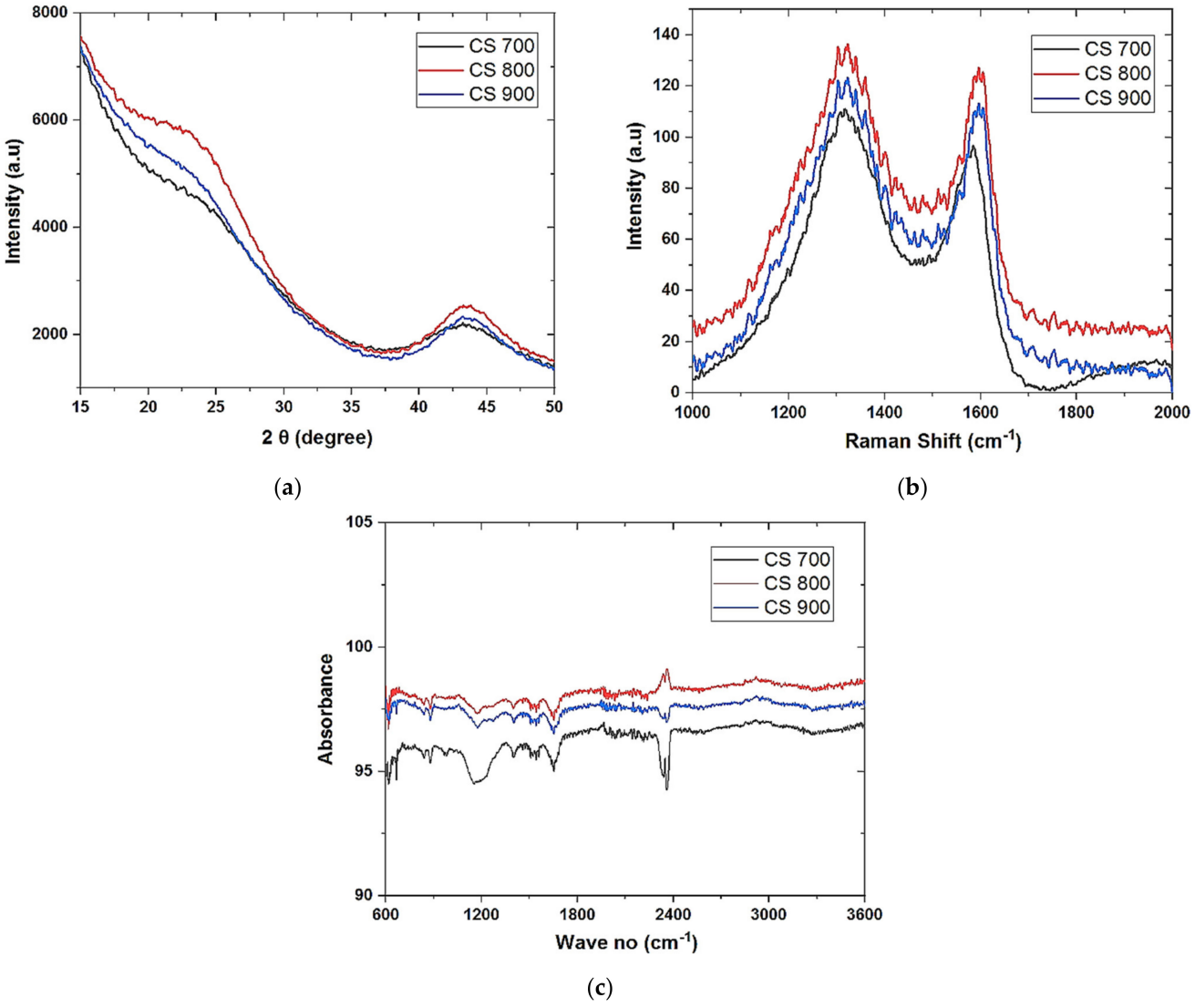

(**a**) (**b**) (**c**)

Figure 2. XRD (**a**) CS 700, CS 800, and CS 900; (**b**) Raman spectra of CS 700, CS 800, and CS 900; (**c**) FTIR of CS 700, CS 800, and CS 900.

Table 1. Interlayer spacing and microcrystallite size with reference to temperature.

Sample	d 002 (nm)	100/101 (nm)	Lc (nm)	La (nm)	Lc/La	Np (Lc/d002)
CS 700	0.37	0.21	6.14	0.80	7.67	16.59
CS 800	0.37	0.21	6.14	0.76	8.07	16.59
CS 900	0.38	0.21	6.51	0.72	9.04	17.13

Using the Debye–Scherrer equation, (D = K/c, a cos), where K is the constant value of 0.9 for Lc (the stack height determined from the 002 plane) and 1.84 for La (the stack width determined from the 100/101 plane), is the XRD machine radiation (0.1541 nm), is the full width at half maximum of the diffraction peak in radian and is the diffraction angle in radian. The ratio of Lc/La corresponds to the relative density of the edge and basal planes of the microcrystallites while Np represents the ratio of plane numbers present in the microcrystallites [28,29]. The size of micro-crystallite in the CS appears to be unaffected by pyrolysis temperature. Additional information on the XRD of the activated carbon may be found in the additional information section of Figure 2a.

3.3. Raman Studies

The influence of temperature and defect on the structural deformation of the carbon lattice was verified using Raman. Because of in-plane vibration, carbonaceous materials show well-defined peaks at the D-band of 1350 cm^{-1} corresponding to disordered graphite and the G-band of 1580 cm^{-1} corresponding to ordered graphite [30]. A defect-free sample has no D band, but our materials have one due to the presence of heteroatoms in the carbon lattice, rendering it insensitive to excitation wavelength [30]. The materials peaks conform to the aforementioned bands under all situations, as illustrated in Figure 2b. In Raman, the intensity ratio (R = ID/IG) indicates the degree of defect present in any carbon-based substance. As indicated in Table 2, the intensity ratio demonstrates a high level of defect in the carbon spheres, with CS 700 having the lowest level of defect.

Table 2. Different intensity ratios of the materials.

Samples	CS 700	CS 800	CS 900
R	0.92	1.15	1.20

3.4. EDS, FTIR, and XPS Studies

Figure 2c shows how FTIR was used to analyze the surface chemistry of CS. The presence of C=C aromatic bonds in the materials is revealed by the identified signal at 1575 cm^{-1}. The –OH stretching vibration of the alcohol and CH3 bands is related with the peaks at 3417 and 2925 cm^{-1}, respectively [31]. The vibrational peaks at 1720.49 cm^{-1} are caused by the C=O carbonyl group, and they are most evident in CS 700, probably due to more carbonyl groups being formed at this pyrolysis temperature. C–H stretching causes the peak at 1382 cm^{-1}, while C–O bonds from esters and ethers cause the peak at 1022 cm^{-1} [32].

Further investigation was carried out using X-ray photoelectron spectroscopy analysis. Information about CS (700, 800, and 900 °C) is presented in Figure 3a,d while that of activated carbon sphere (ACS) is provided in Supplementary Information in Figure S2b. Information regarding EDX is provided in Supplementary Information Table S1.

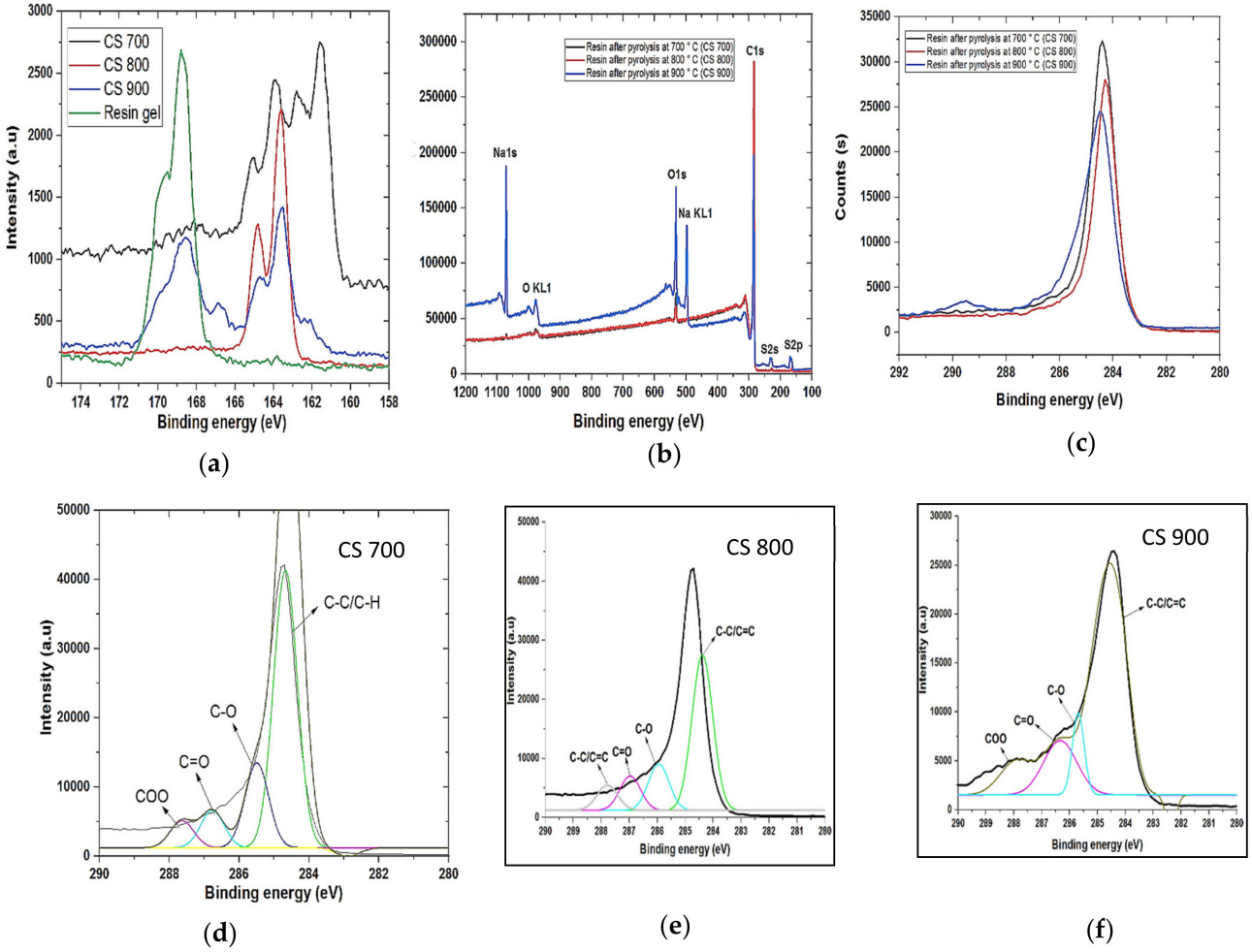

Figure 3. Sulphur 2p spectra of (**a**) resin gel, CS 700, CS 800, and CS 900; (**b**) Whole XPS spectra of CS 700, CS 800, and CS 900; (**c**) C1s spectra of CS 700, CS 800, and CS 900. (**d**–**f**) Deconvoluted C1s spectra of CS 700, CS 800, and CS 900.

The surface elemental atomic compositions of the polymer resin gel before pyrolysis were characterized to be 74.30% C and 19.53% O. After pyrolysis, CS does not show significant difference at all temperatures except for CS 900 with 71.55% C and 17.51% O (highest peak intensity for O element in Figure 3b while CS 700 possessed (95.69% C, 4.31% O) and CS 800 (97.54% C, 2.46% O)). Figure 3a shows the changes in the XPS spectra of Sulphur 2p of both the precursor and the resulting carbons. The XPS research revealed that at temperatures of 700 °C and 800 °C, the sulphonic acid functional group decomposes rapidly to SO_2 and H_2O gases, whereas at higher temperatures of 900 °C, only a little base of the polymer is pyrolyzed, accounting for the large number of O in CS 900. Figure 3b shows that the polymer resin's benzene sulfonic acid band ($C_6H_5SO_3H$), which has an S2p binding energy of 168.8 eV, is present in CS 900 after pyrolysis—though in a less pronounced form than the precursory material—but is absent in CS 700 and CS 800, indicating that CS 900 retains some benzene sulphonic group at this temperature. The peak at 164.0 eV corresponds to phenyl sulfide polymer (C_6H_5S) n [33].

Presence of oxygenated functional groups—i.e., -C=O, COOH, etc.—is beneficial for improvement of electrochemical properties in EDL capacitors as both wettability and hydrophilicity of the capacitor surface is improved [9]. As shown in Figure 3c,d, binding energies of 284.9, 286.7, and 288.9 eV present in the distribution of the peaks correspond to -C-C- carbon bonds, -C-O- carbon bonds, C=O and -COO- (carbonyl and carboxylic peaks) respectively [34].

3.5. Textural Properties

The textural features of carbon spheres produced and activated at various temperatures were compared in this study. The specific surface area of the synthesized carbon spheres decreased sharply as temperature increased, as shown in Table 3, and the lowest temperature (700 °C) appears to be the best temperature for abundant pores development in the resultant carbon. Following that, the selected carbon (CS 700) was activated, and the CS activated at 0.1 M had the highest specific surface area among its counterparts, indicating that a generation of active species was required for pore activation by the activating agent, resulting in a higher specific surface area. All of the electrode materials' isotherm curves had a typical type II adsorption isotherm [35], as illustrated in Figure 4a. The pores accessible for a molecule or ions of a specific size and shape are indicated by the pore size distribution. The pore size distribution of the materials was computed using the BJH model, and it was discovered that the mesopore area is responsible for adsorption (11–30 nm), as shown in Figure 4b. Table 3 summarizes material parameters such as total pore volume, BET specific surface area, and mesopore volume.

Table 3. Textural parameters of CS 700, CS 800, CS 900, ACS 700−0.1, ACS 700−0.3, and ACS 700−0.5.

Sample	V_t ($cm^3 \cdot g^{-1}$)	S_{BET} ($m^2 \cdot g^{-1}$)	V_{MESO} ($cm^3 \cdot g^{-1}$)
CS-700	0.65	811.96	0.43
CS-800	0.62	778.75	0.40
CS-900	0.56	654.57	0.41
ACS 700−0.1	0.68	849.18	0.48
ACS 700−0.3	0.66	812.74	0.47
ACS 700−0.5	0.66	798.82	0.46

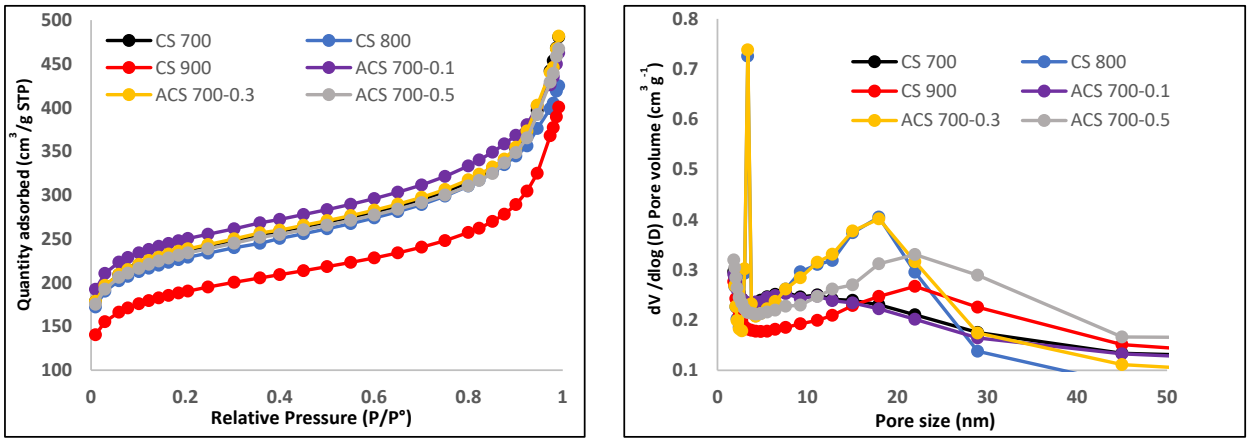

(a) (b)

Figure 4. (**a**) Nitrogen adsorption–desorption isotherm of CS 700, CS 800, CS 900, ACS 700−0.1, ACS 700−0.3, and ACS 700−0.5. (**b**) Pore width distribution of CS 700, CS 800, CS 900, ACS 700−0.1, ACS 700−0.3, and ACS 700−0.5.

3.6. Electrochemical Studies

Figure 5 shows the Nyquist plots of the EIS data of the materials (a). Figure 5 shows the effect of changing the pyrolysis temperature on the semi-circle formation and Warburg diffusion lines of these materials (a). The dominant resistive nature of the material is depicted by a tiny semicircle in the high frequency range.

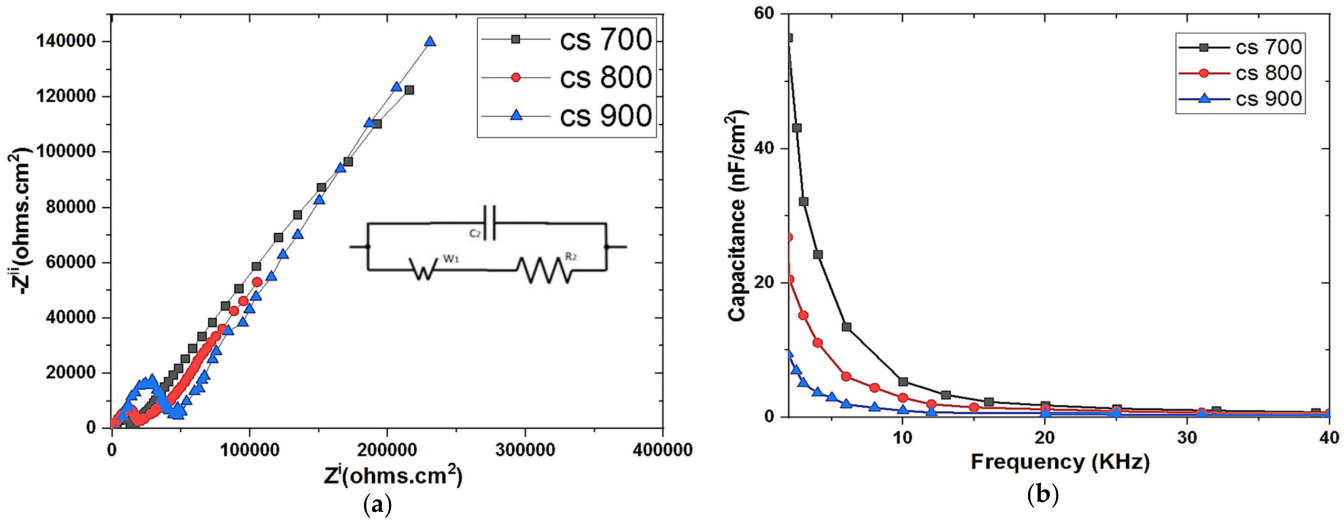

Figure 5. Nyquist plot of (**a**) CS 700, 800, and 900 respectively; (**b**) theoretical capacitance of CS 700, CS 800, and CS 900 as a function of frequency.

Solution resistance (Rs) is the resistance of the solution or electrolyte in use and indicates the start of the semicircle line at Z^i (left intercept at real axis) in EIS. The electrode internal or intrinsic resistance (R) marks the semicircle's end or termination (right intercept at Z^i real axis). The ease with which ions diffuse into the pores of the electrode or material is represented by Warburg diffusion in the intermediate frequency range, whilst the capacitive behavior of the material is shown in the low frequency range. Pyrolysis at 700 °C appears to be the exact optimal temperature for generating CS with the lowest resistivity, as indicated in Table 4.

Table 4. EIS parameters from Nyquist plots calculated theoretically from equivalent circuit fitting.

Sample	R_2 (KΩ.cm^2)	Yo (μS)	Capacitance (nF)
CS 700	12.59	22.99	0.467
CS 800	19.87	53.19	0.380
CS 900	35.00	06.22	0.361
ACS 700−0.1	3.33	2.83	1.780
ACS 700−0.3	23.79	1.88	0.106
ACS 700−0.5	9.34	21.60	0.185

R: Resistance, Yo: Warburg diffusion.

The theoretical capacitance determined as a function of frequency from the imaginary portion (Z^{ii}) of the EIS data of the synthesized carbons was shown in Figure 5b. The CS 700 capacitance increases as the frequency range is increased. This indicates that ions migrate more easily or penetrate more deeply into the pores (intrapores) of the CS-700, resulting in a considerable differential in capacitance. CS 700 also has the lowest resistance (Table 4), which allows for efficient ion transport and rapid diffusion into its pores, resulting in the maximum capacitive behavior.

CS 700 was chosen as a desired candidate of interest because it has the lowest resistivity value and the highest capacitance, and it was chemically activated to improve its surface charge using FeCl3 of various concentrations.

To validate the effect of varied concentrations of activating agent on the resistivity and capacitance of the CS-700, EIS analysis was done (Figure S3), and as indicated in Table 4, ACS 700−0.1 has the lowest resistance and highest capacitance.

Galvanostatic Charge–Discharge and Cyclic Voltammetry

The reversibility of the carbon electrodes was tested using a galvanostatic charge-discharge (GCD) technique. The symmetrical triangular forms of GCD without any type of

variation, as shown in Figure 6a, clearly suggest that the storage mechanism is predominantly EDL in nature and that all electrodes are reversible [36]. Figure 6a demonstrates that CS 700 has the largest area of size, indicating that it performs at a fast rate.

Cyclic voltammetry (CV) is an important tool in predicting the capacitive behavior of a capacitor. For an EDL capacitor, an almost or a rectangular shape is observed as a function of scan rates. For an ideal EDL capacitor, a rectangular shape depicts low resistivity of ions diffusion to the pores of the material thus enabling the formation of stable EDL interface especially at a low scan rate [6]. The capacitive behavior of the materials is shown in Figure 6b,d. Although all of the samples have pseudo-rectangular shapes indicating the low capacitive characteristics of these materials, CS 700 exhibited the most stable EDL formation out of all of them, possibly due to its improved surface chemistry and generation of electroactive species at this optimal pyrolysis temperature, leading to higher ions diffusion as shown in Figure 6b with highest current area under CV. Following activation, a modest concentration of 0.1 M $FeCl_3$ is all that is required to improve electrochemical behavior, as seen in Figure 6d. The addition of iron (Fe) at this concentration must have increased the material's carbon conductivity network (surface charge), resulting in decreased resistivity at the electrode–electrolyte interface. After activation, the curves of the materials take on a considerable form, going from pseudo-rectangular to almost rectangular at the same scan rate (50 mV s^{-1}). This demonstrates the effectiveness of the activation procedure. Table 5 shows the predicted EDL capacitance of all carbon electrodes based on the absolute value of the slopes in Figure 6c,e.

Table 5. Electrical double layer capacitance (C_{EDL}) calculated from the charge and discharge currents of the CV curves of the synthesized carbons in aqueous solution.

Sample	CS 700	CS 800	CS 900	ACS 700−0.1	ACS 700−0.3	ACS 700−0.5
C_{EDL} (μF cm^{-2})	5.10	4.50	2.90	9.00	5.00	4.20

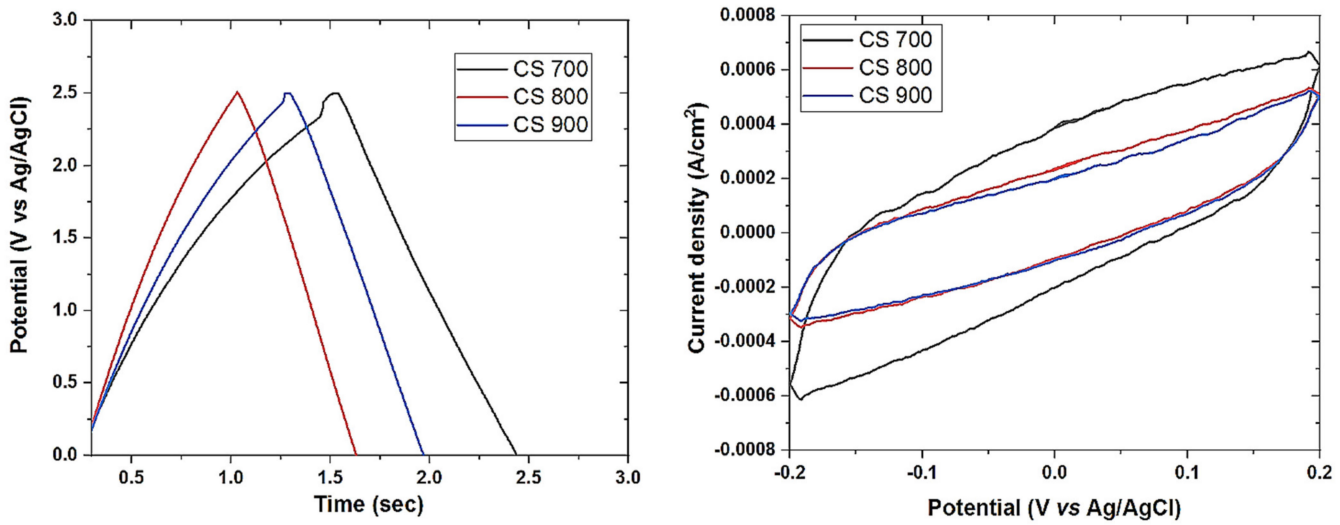

(a) (b)

Figure 6. *Cont.*

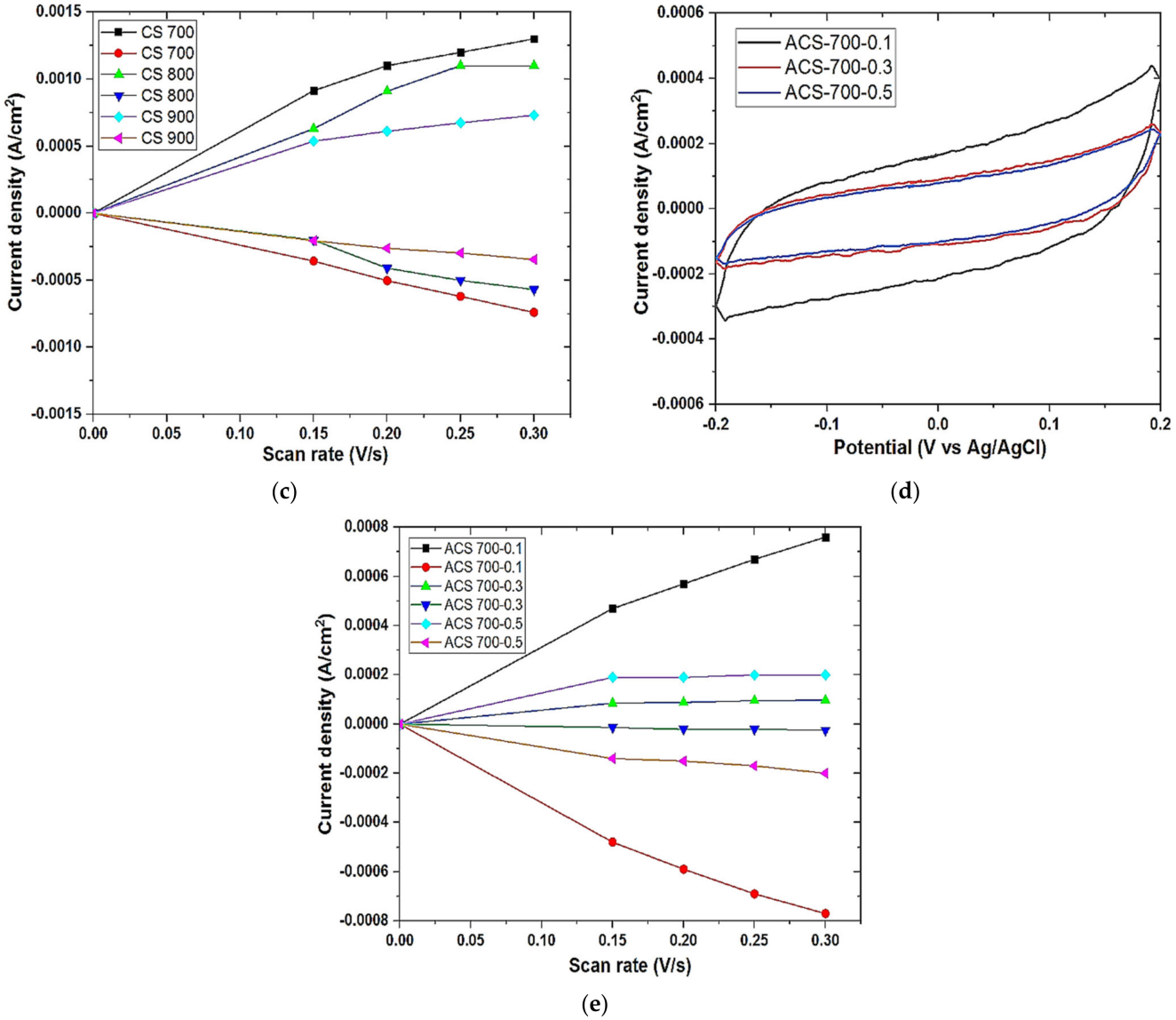

Figure 6. Galvanostatic charge–discharge (**a**) of CS 700, CS 800, and CS 900; (**b**,**d**) cyclic voltammetry curve of CS 700, CS 800, CS 900, ACS 700−0.1, ACS 700−0.3, and ACS 700−0.5 at the scan rates of 50 mV/s respectively; (**c**,**e**) double-layer capacitance voltammetry measurements of CS 700, CS 800, CS 900, ACS 700−0.1, ACS 700−0.3, and ACS 700−0.5 respectively. Cyclic voltammetry measurements were carried out in 1 M NaCl aqueous electrolyte and measured in a non-Faradaic region of the voltammogram at high scan rates of 150–300 mV s^{-1}. The charging current (ref current density above 0 A cm^{-2}) and discharging current (ref. current density below 0 A/cm^2) were plotted as a function of scan rate (V s^{-1}). The determined double-layer capacitance of the system was taken as the absolute value of the slope fits to the data [36].

Our materials' double layer capacitance values are consistent with those reported in the literature—i.e., for carbon materials such as carbon black, the reported double layer capacitance ranges from 4 to 10 F cm^{-2}, while for activated carbon, it ranges from 10–15 F cm^{-2} [37–39]. Table 6 shows the double layer capacitance of several carbon compounds based on published data [40,41].

Table 6. Values of electrochemical double layer capacitance of carbonaceous materials as found in literature.

Carbonaceous Material	Electrolyte	Double Layer Capacitance ($\mu F\ cm^{-2}$)	Ref.
Carbon black	10% NaCl	19.00	[42]
	1 M H_2SO_4	8.00	[42]
	31 wt% KOH	9.00	[42]
Carbon fiber cloth	0.5 M Et_4NbF_4	6.90	[42]
Graphite powder	10% NaCl	35.00	[42]
Graphite cloth	0.168 N NaCl	10.70	[42]
Glassy carbon	0.9 N NaF	13.00	[42]
Carbon aerogel	4 M KOH	23.00	[42]
ACS	1 M NaCl	9.00	This work

ACS: activated carbon sphere.

4. Conclusions and Future Perspectives

Pyrolysis of polymeric beads in a tube furnace at various heating temperatures yielded spherical carbons in this work. Carbon spheres synthesized at 700 °C had the best electrochemical characteristics and the most spherical form of all the carbon spheres tested. As a result, iron, which acts as an activator at this pyrolysis temperature, replaced the precursor gel (cation exchange resin). It was proven that the activation state is dependent on the activator concentration. When compared to the results reported in the literature on its use as an electrical double layer capacitor, the produced activated carbon demonstrated good electrochemical properties. This demonstrates that this easy and effective approach of obtaining spherical carbon from a low-cost polymer source is a promising technology for electrochemical capacitor (EC) manufacture.

We believe that a well-controlled polymerization technique, such as the RAFT approach, can be a focus of research for easy scale-up of self-supporting carbon synthesis from polymers, as well-oriented and structured carbons can be created for applications as EDL capacitors from this method. Additionally, research into conductive polymers such as poly (3,4-ethylenedioxythiophene)—poly (styrene sulfonic acid) (PEDOT-PSS), which has a low resistance, could be advantageous. They are also stable in water and, thanks to their hydrophobic carbon chain, can potentially create carbon. Furthermore, more research is needed to determine the viability of employing water soluble polymers as a carbon source for EC, however recent findings from various groups demonstrate that PEDOT-PSS has the potential to increase performance [42–44].

Supplementary Materials: The following are available online at https://www.mdpi.com/article/10.3390/c7040082/s1, Figure S1: SEM micrographs of (a) ACS 700−0.1 (b) ACS 700−0.3 (c) ACS 700−0.5; Figure S2: (a) XRD of ACS 700−0.1, ACS 700−0.3, and ACS 700−0.5; (b) XPS spectra of Fe 2p of ACS 700−0.1, ACS 700−0.3, and ACS 700−0.5; Figure S3: Nyquist plot of activated CS 700 at 0.1 M (ACS 700−0.1), 0.3 M (ACS 700−0.3), and 0.5 M (ACS 700−0.5) $FeCl_3$. Table S1: Elemental composition of CS obtained from pyrolysis of polymer resin at 700, 800, and 900 °C.

Author Contributions: Conceptualization, G.B.F.; Methodology, G.B.F.; Software, G.B.F.; Validation, G.B.F., A.E., N.C.A. and R.C.E.; Formal analysis, G.B.F.; Investigation, G.B.F.; Resources, G.B.F. and A.E.; Data curation, G.B.F. and N.C.A.; Writing—G.B.F., Visualization, G.B.F.; Supervision, G.B.F., A.E. and R.C.E.; Project administration, G.B.F.; Funding acquisition, G.B.F. All authors have read and agreed to the published version of the manuscript.

Funding: This research was funded by the Federal Government of Nigeria through Tertiary Education Trust fund (TETFUND) and Campus France (CF) for the Ph.D. funding of Gbenro Folaranmi with the funding number CAMPUS FRANCE 914886H and European Institute of Membranes (IEM).

Institutional Review Board Statement: Not applicable.

Informed Consent Statement: Not applicable.

Acknowledgments: Special thanks to Institute European des Membranes (IEM), TETFUND and all the technologists involved in this work.

Conflicts of Interest: The authors declare no conflict of interest.

References

1. Zhang, L.L.; Zhao, X.S. Carbon-based materials as supercapacitor electrodes Chem. *Soc. Rev.* **2009**, *38*, 2520. [CrossRef]
2. Simon, P.; Gogotsi, Y. Materials for electrochemical capacitors. *Nat. Mater.* **2008**, *7*, 845. [CrossRef]
3. Wang, G.; Zhang, L.; Zhang, J. A review of electrode materials for electrochemical supercapacitors. *Chem. Soc. Rev.* **2012**, *41*, 797–828. [CrossRef] [PubMed]
4. Titirici, M.M.; Antonietti, M. Chemistry and materials options of sustainable carbon materials made by hydrothermal carbonization. *Chem. Soc. Rev.* **2010**, *39*, 103. [CrossRef] [PubMed]
5. Mora, E.; Blanco, C.; Pajares, J.A.; Santamaría, R.; Menéndez, R. Chemical activation of carbon mesophase pitches. *J. Colloid Interface Sci.* **2006**, *298*, 341–347. [CrossRef] [PubMed]
6. Folaranmi, G.; Bechelany, M.; Sistat, P.; Cretin, M.; Zaviska, F. Towards Electrochemical Water Desalination Techniques: A Review on Capacitive Deionization, Membrane Capacitive Deionization and Flow Capacitive Deionization. *Membranes* **2020**, *10*, 96. [CrossRef] [PubMed]
7. Wang, X.Q.; Wang, P.; Ning, P.; Ma, X.Y.; Wang, F.; Guo, X.L.; Lan, Y. Adsorption of gaseous elemental mercury with activated carbon impregnated with ferric chloride. *RSC Adv.* **2015**, *5*, 24899. [CrossRef]
8. Bonvin, F.; Jost, L.; Randin, L.; Bonvin, E.; Kohn, T. Super-fine powdered activated carbon (SPAC) for efficient removal of micropollutants from wastewater treatment plant effluent. *Water Res.* **2016**, *90*, 90–99. [CrossRef] [PubMed]
9. Folaranmi, G.; Bechelany, M.; Sistat, P.; Cretin, M.; Zaviska, F. Comparative Investigation of Activated Carbon Electrode, and a Novel Activated Carbon/Graphene Oxide Composite Electrode for an Enhanced Capacitive Deionization. *Materials* **2020**, *13*, 5185. [CrossRef]
10. Zhang, D.Y.; Hao, Y.; Zheng, L.W.; Ma, Y.; Feng, H.X.; Luo, H.M. Nitrogen and sulfur co-doped ordered mesoporous carbon with enhanced electrochemical capacitance performance. *J. Mater. Chem. A* **2013**, *1*, 7584. [CrossRef]
11. Huo, S.L.; Liu, M.Q.; Wu, L.L.; Liu, M.J.; Xu, M.; Ni, W.; Yan, Y.M. Methanesulfonic acid-assisted synthesis of N/S co-doped hierarchically porous carbon for high performance supercapacitors. *J. Power Sources* **2018**, *387*, 81. [CrossRef]
12. Cheng, L.L.L.; Hu, Y.Y.; Qiao, D.D.; Zhu, Y.; Wang, H.; Jiao, Z. One-step radiolytic synthesis of heteroatom (N and S) co-doped graphene for supercapacitors. *Electrochim. Acta* **2018**, *259*, 587. [CrossRef]
13. Falco, C.; Marco-Lozar, J.P.; Salinas-Torres, D.; Morallón, E.; Cazorla-Amorós, D.; Titirici, M.M.; Lozano-Castelló, D. Tailoring the porosity of chemically activated hydrothermal carbons: Influence of the precursor and hydrothermal carbonization temperature. *Carbon* **2013**, *62*, 346. [CrossRef]
14. Mao, L.; Zhang, Y.; Hu, Y.; Hung, H.K.; Ke, Q.; Liu, H.; Hu, Z.; Zhao, D.; Wang, J. Activation of sucrose-derived carbon spheres for high-performance supercapacitor electrodes. *RSC Adv.* **2015**, *5*, 9307–9313. [CrossRef]
15. Lv, Y.; Chen, J.; Jia, W.; Wu, X.; Guo, J.; Ding, L.; Jia, D.; Tong, F. N/S co-doped coal-based porous carbon spheres as electrode materials for high performance supercapacitors. *RSC Adv.* **2020**, *10*, 11033–11038. [CrossRef]
16. Wickramaratne, N.P.; Jaroniec, M. Activated Carbon Spheres for CO_2 Adsorption. *ACS Appl. Mater. Interfaces* **2013**, *5*, 1849–1855. [CrossRef] [PubMed]
17. Shen, C.; Yu, J.; Li, P.; Grande, C.A.; Rodrigues, A.E. Capture of CO_2 from flue gas by vacuum pressure swing adsorption using activated carbon beads. *Adsorption* **2010**, *17*, 179–188. [CrossRef]
18. Zeng, Y.; Wang, K.; Yao, J.; Wang, H. Hollow carbon beads for significant water evaporation enhancement. *Chem. Eng. Sci.* **2014**, *116*, 704–709. [CrossRef]
19. Zeng, Y.; Wang, K.; Yao, J.; Wang, H. Hollow carbon beads fabricated by phase inversion method for efficient oil sorption. *Carbon* **2014**, *69*, 25–31. [CrossRef]
20. Singh, G.; Kim, I.Y.; Lakhi, K.S.; Srivastava, P.; Naidu, R.; Vinu, A. Single step synthesis of activated bio-carbons with a high surface area and their excellent CO_2 adsorption capacity. *Carbon* **2017**, *116*, 448–455. [CrossRef]
21. Singh, G.; Lakhi, K.S.; Kim, I.Y.; Kim, S.; Srivastava, P.; Naidu, R.; Vinu, A. Highly Efficient Method for the Synthesis of Activated Mesoporous Biocarbons with Extremely High Surface Area for High-Pressure CO_2 Adsorption. *ACS Appl. Mater. Interface* **2017**, *9*, 29782–29793. [CrossRef] [PubMed]
22. Singh, A.; La, D. Preparation and characterization of activated carbon spheres from polystyrene sulphonate beads by steam and carbon dioxide activation. *J. Appl. Polym. Sci.* **2010**, *115*, 2409–2415. [CrossRef]
23. He, P.; Haw, K.-G.; Yan, S.; Tang, L.; Fang, Q.; Qiu, S.; Valtchev, V. Carbon beads with a well-defined pore structure derived from ion-exchange resin beads. *J. Mater. Chem. A* **2019**, *7*, 18285. [CrossRef]
24. Wu, D.C.; Hui, C.M.; Dong, H.C.; Pietrasik, J.; Ryu, H.J.; Li, Z.H.; Zhong, M.J.; He, H.K.; Kim, E.K.; Jaroniec, M.; et al. Nanoporous Polystyrene and Carbon Materials with Core-Shell Nanosphere-Interconnected Network Structure. *Macromolecules* **2011**, *44*, 5846. [CrossRef]
25. Ouyang, Y.; Shi, H.; Fu, R.; Wu, D. Highly Monodisperse Microporous Polymeric and Carbonaceous Nanospheres with Multifunctional Properties. *Sci. Rep.* **2013**, *3*, 1430. [CrossRef]

26. Liang, Y.; Chen, L.; Zhuang, D.; Liu, H.; Fu, R.; Zhang, M.; Wu, D.; Matyjaszewski, K. Fabrication and nanostructure control of super-hierarchical carbon materials from heterogeneous bottlebrushes. *Chem. Sci.* **2017**, *8*, 2101. [CrossRef]
27. Lee, W.H.; Moon, J.H. Monodispersed N-Doped Carbon Nanospheres for Supercapacitor Application. *ACS Appl. Mater. Interfaces* **2014**, *6*, 13968. [CrossRef]
28. Valante-Nabais, J.M.; Teixeira, J.G.; Almeida, I. Development of easy made low cost bindless monolithic electrodes from biomass with controlled properties to be used as electrochemical capacitors. *Bioresour. Technol.* **2011**, *102*, 2781–2787. [CrossRef] [PubMed]
29. Farma, R.; Deraman, M.; Awitdrus, A.; Talib, I.A.; Taer, E.; Basri, N.H.; Manjunatha, J.G.; Ishak, M.M.; Dollah, B.N.M.; Hashmi, S.A. Preparation of highly porous binderless activated carbon electrodes from fibres of oil palm empty fruit bunches for application in supercapacitors. *Bioresour. Technol.* **2013**, *132*, 254–261. [CrossRef] [PubMed]
30. Qiang, D.; Gang, W.; Bingqing, Q.; Chao, H.; Yuwei, W.; Jieshan, Q. Electrospun composites made of reduced graphene oxide and activated carbon nanofibers for capacitive deionization. *Electrochim. Acta* **2014**, *137*, 388–394.
31. Ng, E.P.; Mintova, S. Quantitative moisture measurements in lubricating oils by FTIR spectroscopy combined with solvent extraction approach. *Micro. Chem. J.* **2011**, *98*, 177–185. [CrossRef]
32. Feng, W.; He, P.; Ding, S. Oxygen-doped activated carbons derived from three kinds of biomass: Preparation, characterization, and performance as electrode materials for supercapacitors. *RSC Adv.* **2016**, *6*, 5949–5956. [CrossRef]
33. Bamford, C.H.; Tipper, C.F.H. *Comprehensive Chemical Kinetics, Volume 14: Degradation of Polymers*; Elsevier: Amsterdam, The Netherlands, 1975; Chapter 1.
34. Alabadi, A.; Razzaque, S.; Yang, Y.; Chen, S.; Tan, B. Highly porous activated carbon materials from carbonized biomass with high CO_2 capturing capacity. *Chem. Eng. J.* **2015**, *281*, 606–612. [CrossRef]
35. Basri, N.H.; Dolah, B.N.M. Physical and electrochemical properties of supercapacitor electrodes derived from carbon nanotube and biomass carbon. *Int. J. Electrochem. Sci.* **2013**, *8*, 257–273.
36. Liang, Z.; Xia, H.; Liu, H.; Zhang, L.; Zhou, J.; Li, H.; Xie, W. Enhanced capacitance characteristic of microporous carbon spheres through surface modification by oxygen-containing groups. *Results Phys.* **2019**, *15*, 102586. [CrossRef]
37. McCrory, C.C.L.; Jung, S.; Peters, J.C.; Jaramillo, T.F. Benchmarking Heterogeneous Electrocatalysts for the Oxygen Evolution Reaction. *J. Am. Chem. Soc.* **2013**, *135*, 16977–16987. [CrossRef]
38. Cheng, J.; Minett, A.; Liu, Y.; Lynam, C.; Sherrell, P.; Wang, C.; Wallace, G.G. Direct Growth of Flexible Carbon Nanotube Electrodes. *Adv. Mater.* **2008**, *20*, 566. [CrossRef]
39. Li, H.; Wang, Z.; Chen, L.; Huang, X. Research on Advanced Materials for Li-ion Batteries. *Adv. Mater.* **2009**, *21*, 4593. [CrossRef]
40. Reimers, J.N.; Dahn, J.R.; von Sacken, U. Effects of Impurities on the Electrochemical Properties of $LiCoO_2$. *J. Electrochem. Soc.* **1993**, *140*, 2752. [CrossRef]
41. Ji, H.; Xin, Z.; Qiao, Z.; Jung, J.; Zhu, Y.; Lu, Y.; Zhang, L.L.; MacDonald, A.H.; Ruoff, R.S. Capacitance of carbon-based electrical double-layer capacitors. *Nat. Commun.* **2014**, *5*, 3317. [CrossRef]
42. Lei, C.; Wilson, P.; Lekakou, C. Effect of poly(3,4-ethylenedioxythiophene) (PEDOT) in carbon-based composite electrodes for electrochemical supercapacitors. *J. Power Sources* **2011**, *196*, 7823–7827. [CrossRef]
43. Yoon, D.H.; Yoon, S.H.; Ryu, K.S.; Park, Y.H. PEDOT: PSS as multi-functional composite material for enhanced Li-air-battery air electrodes. *Sci. Rep.* **2016**, *6*, 19962. [CrossRef] [PubMed]
44. Gallegos, A.K.C.; Rincón, M. Carbon nanofiber and PEDOT-PSS bilayer systems as electrodes for symmetric and asymmetric electrochemical capacitor cells. *J. Power Sources* **2006**, *162*, 743–747. [CrossRef]